Mesoporous Anodes

DOI: 10.1002/ange.200907099

Lithium Intercalation into Mesoporous Anatase with an Ordered 3D Pore Structure**

*Yu Ren, Laurence J. Hardwick, and Peter G. Bruce**

There is a great deal of interest in TiO_2 nanoparticles, nanowires and nanotubes due to their potential advantages (safety, rate) as anodes replacing graphite in a new generation of rechargeable lithium batteries.[1,2] Here we report the synthesis of mesoporous anatase with an ordered 3D pore structure, using a hard template, and investigate its properties as a lithium intercalation host. It exhibits a hierarchical pore structure. Despite being composed of micrometer sized particles, the ordered mesoporous morphology inside the particles results in a high Li storage capacity and high rates of intercalation, with the material exhibiting an energy density between 30 and 200% higher than the best high rate performance reported to date for any titanate (6 nm nanoparticle anatase).[1b] It has been proposed that the reason nanoparticles such as anatase and $LiFePO_4$ exhibit facile Li insertion is the ability of such particles to transform spontaneously for one phase to the other, i.e., a particle is either phase A or B but not both.[1c,3] The micrometer sized mesoporous particles cannot do so but still show facile intercalation. This is related to the ease with which the strain of transforming between the anatase (phase A) and the orthorhombic $Li_{0.59}TiO_2$ structures (phase B) is accommodated within the thin (6.5 nm) walls on intercalation.

Mesoporous anatase with an ordered 3D pore structure was synthesized using the silica KIT-6 as a hard template (see experimental section). The ordered pore structure is evident in the TEM data (Figure 1 A,B) and replicates that of the KIT-6 hard template with space group *Ia3d*. An a_0 lattice parameter for the mesostructure of 23.3 nm was extracted from the data. The mesoporous structure is preserved throughout as demonstrated by examining many particles. The walls (6.5 nm) are composed of anatase crystallites. A lattice spacing of 0.350 nm was observed in HRTEM (Figure 1 B), in good agreement with the *d*-spacing of 0.352 nm associated with the (101) direction of anatase (ICDD 00-001-5062). The low and wide-angle PXRD data are shown in Figure 2. The low-angle diffraction patterns exhibit one relatively sharp peak below 1°, which could be indexed as the 211 reflection in the *Ia3d* space group, corresponding to an a_0 lattice parameter of 23.5 nm in good agreement with the TEM data. The broad peaks in the wide-angle PXRD for the as-prepared mesoporous material are in good agreement with those for anatase nanoparticles, AK-1 (Bayer) (Figure 2 A). The mesoporous anatase peak widths are greater than those of the nanoparticles in accord with the walls being thinner than the diameter of the nanoparticles (15 nm).

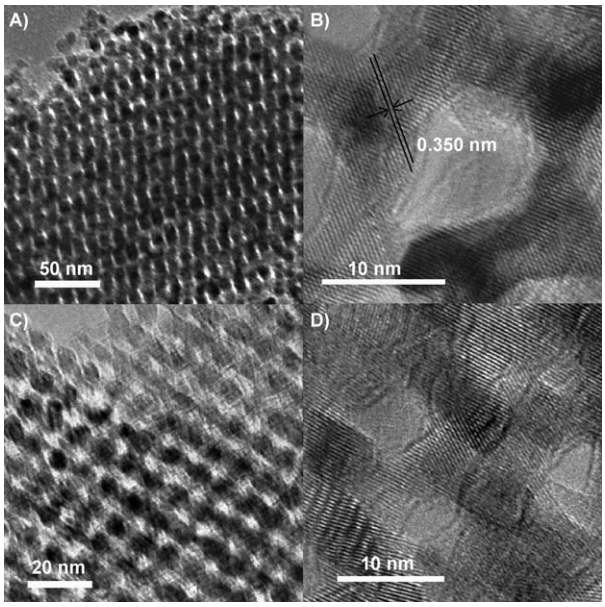

Figure 1. TEM and HRTEM data for ordered mesoporous anatase: A,B) as-prepared; C,D) after 1000 cycles (12000 mA g^{-1}).

The mesostructures were investigated further by N_2 sorption measurements. Typical type IV isotherms exhibiting H_2 hysteresis were observed (Supporting Information, Figure S1a), consistent with the mesoporosity evident in the TEM and low-angle PXRD data. BJH pore size distributions exhibit at least three peaks, demonstrating a hierarchical pore structure. A well resolved narrow peak centered at 5 nm, a peak at approximately 11 nm and a third broad peak at ca. 50 nm (Figure S1b). The first peak corresponds to the mesopores observed by TEM in Figure 1. The second arises because KIT-6 has two interpenetrating sets of pores connected by microporous bridges. In regions where the bridges are complete, both pores will be filled and the replica TiO_2 is composed of the 5 nm pores. Where the bridges are incomplete and only one set of KIT-6 pores are filled, the replica exhibits 11 nm pores (Figure S2a). Such a phenomenon had been discussed previously for other KIT-6 templated materials.[4] The third peak corresponds to interparticle voids. The 11

[*] Y. Ren, Dr. L. J. Hardwick, Prof. P. G. Bruce
School of Chemistry, University of St Andrews
The Purdie Building, North Haugh, St Andrews KY16 9ST (UK)
Fax: (+44) 1334-463-808
E-mail: p.g.bruce@st-andrews.ac.uk

[**] P.G.B. is indebted to the EPSRC (SUPERGEN), the EU for financial support, and Prof. D. Graham, University of Strathclyde, for access to their Raman microscope. Y.R. is indebted to EASTCHEM for a studentship.

Supporting information for this article is available on the WWW under http://dx.doi.org/10.1002/anie.200907099.

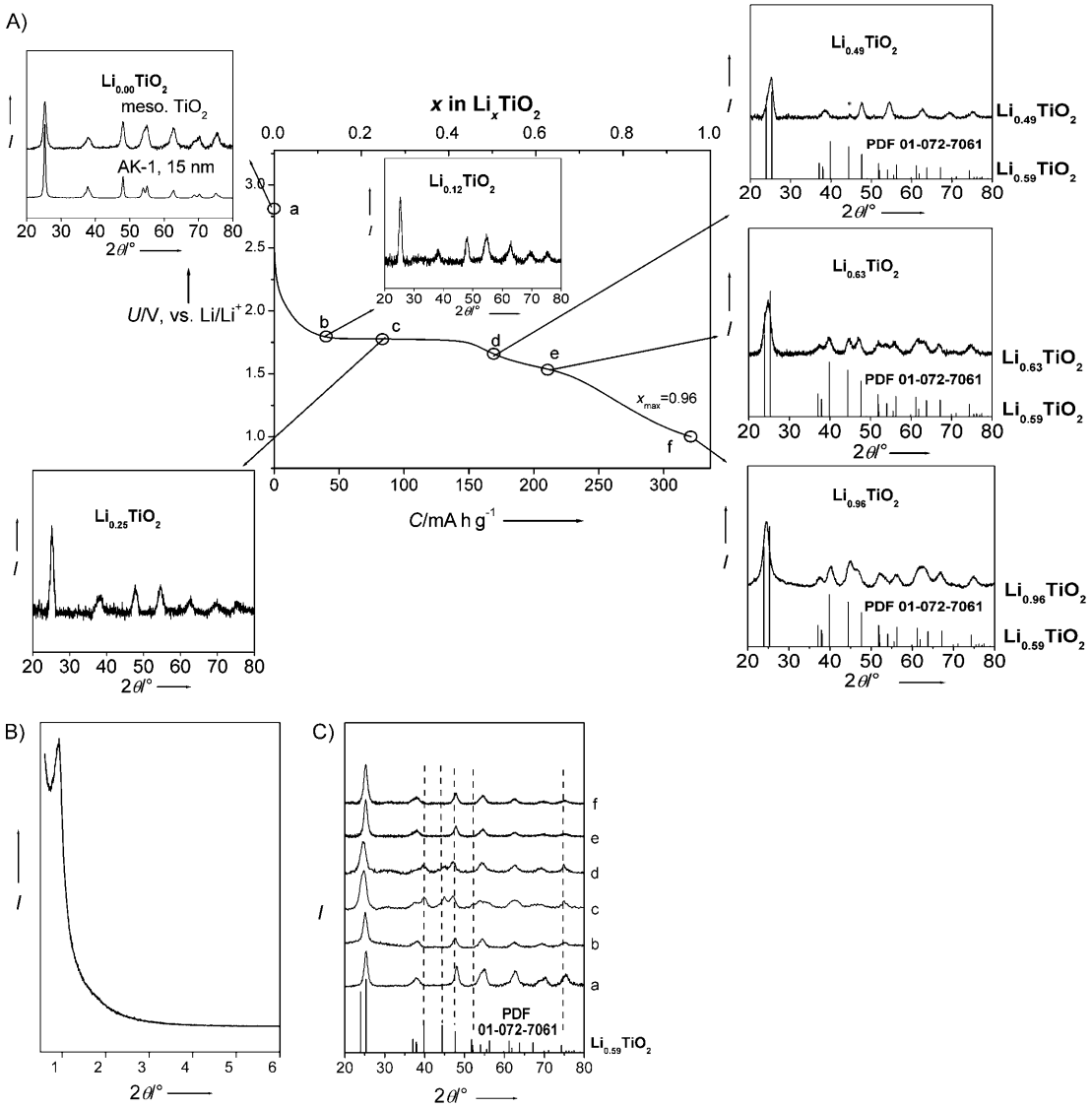

Figure 2. A) Variation of potential on the first discharge (30 mA g^{-1}) and associated ex situ wide-angle PXRD patterns. B) The low-angle PXRD pattern of mesoporous anatase. C) The ex-situ wide-angle PXRD patterns of a) mesoporous anatase, b) mesoporous anatase charged to 3.00 V on the 2nd cycle, discharged to c) 1.5 V and d) 1.0 V after 200 cycles at the rate of 30 mA g^{-1}, charged to 3 V after e) 500 cycles, and f) 1000 cycles at the rate of 12000 mA g^{-1}. Standard of orthorhombic $Li_{0.59}TiO_2$ phase (ICDD No. 01-072-7061) is shown for comparison. Asterisk near 45° is the orthorhombic lithium titanate phase. The PXRD curves are offset for clarity.

and 50 nm voids are seen in the TEM data in Figure S2, providing further evidence for the hierarchical pore structure. The BET surface area is 205 $m^2 g^{-1}$.

The variation of potential on lithium intercalation into mesoporous anatase (discharge) is shown in Figure 2 A along with the PXRD data collected at various points along the curve. The load curve and associated structural changes are similar to those observed for nanoparticulate anatase.[1a,b] A capacity of 322 mA h g^{-1} at 0.09 C (30 mA g^{-1}; note that 1 C = 336 mA g^{-1}) is observed. The potential changes continuously for lithium insertion up to $x = 0.12$ in Li_xTiO_2, in accord with the PXRD data, which suggest retention of the tetragonal anatase structure but with a small volume expansion ($a =$ 3.784, $c = 9.51$ Å for as-prepared mesoporous anatase and $a = 3.797$, $c = 9.455$ Å for $Li_{0.12}TiO_2$). Thereafter the load curve exhibits a plateau up to approximately $x = 0.46$ indicative of a two phase intercalation process. The 101 anatase peak is broadened by 20% at $x = 0.25$, providing some evidence that changes are occurring along the plateau. However, no distinct peaks of a second phase appear until the end of the plateau at $x = 0.49$, at which point the 45° peak associated with the orthorhombic phase is observed. Thereafter orthorhombic $Li_{0.59}TiO_2$ dominates the PXRD and exhibits a continuous lattice expansion up to the maximum intercalation composition of $x = 0.96$. The structural changes associated with the load curve were investigated further by in situ Raman microscopy (Figure 3). The as-prepared tetragonal anatase phase is characterized by a strong peak at 150 cm^{-1} that decreases substantially in intensity on lithium insertion up to $x = 0.05$. Thereafter peaks corresponding to

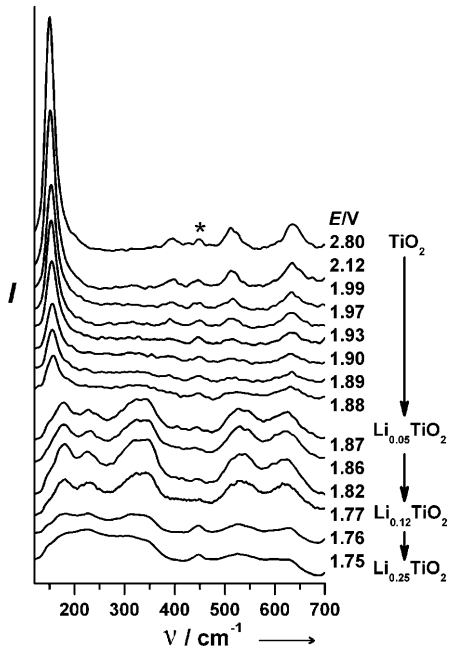

Figure 3. In situ Raman spectral series during lithium insertion into anatase that shows the tetragonal-to-orthorhombic phase change. Spectra were taken at different positions along the discharge curve. Asterisk at 448 cm^{-1} indicates a band originating from the electrolyte. The spectra are offset for clarity.

the orthorhombic phase are clearly evident and dominate the spectrum, in part because of the substantial loss of intensity of the 150 cm^{-1} peak of anatase.[1d] These Raman data demonstrate that the orthorhombic phase begins to grow even before the onset of the plateau. Raman spectroscopy is capable of probing short-range structure not easily observed by PXRD, which more clearly probes long-range order. Taking the Raman, PXRD and electrochemical data together, they indicate that nuclei of the orthorhombic phase begin to form even at $x = 0.05$, but are too small to produce well defined peaks in the PXRD data. The nuclei grow and are evident in PXRD data at the end of the plateau and beyond. Since the PXRD data exhibit expansion of the tetragonal phase up to the plateau onset at $x = 0.1$, we must assume that despite the formation of the orthorhombic phase intercalation into the tetragonal phase continues. It may be that the surfaces of the growing nuclei or there interfaces with the parent, anatase phase, contribute to the free energy of the system and permit a change in the composition of the tetragonal phase. Certainly changes of composition in two-phase regions are not unprecedented, especially for nanomaterials.[1c] However such a hypothesis requires detailed investigation by for example computational methods. Raman data after the onset of the plateau at $x = 0.12$ exhibit increasingly broadened peaks of lower intensity. This loss of intensity of all peaks continues along the plateau. Extraction of lithium reverses these processes which are repeated on subsequent cycling. Charge and discharge curves as a function of rates are shown in Figure S5.

Titanate anodes are employed because of their superior safety and ability to sustain high charge/discharge rates compared with graphite, features that are important for high power applications such as electric vehicles. Therefore we have investigated the rate capability of mesoporous anatase and compared it with the best performance reported for anatase in the literature, which was for 6 nm anatase nanoparticles.[1b] Electrodes were prepared identically with the same mass loading of active material and the same 15 wt.% of carbon. However, in the case of the nanoparticulate anatase material, additional electrodes were constructed with 45 wt.% of carbon (TiO_2:SuperS:Kynar = 50:40:5) corresponding to the composition used in the literature report for 6 nm nanoparticulate anatase that showed the highest rate capability so far.[1b] The results are reported in Figure 4 where

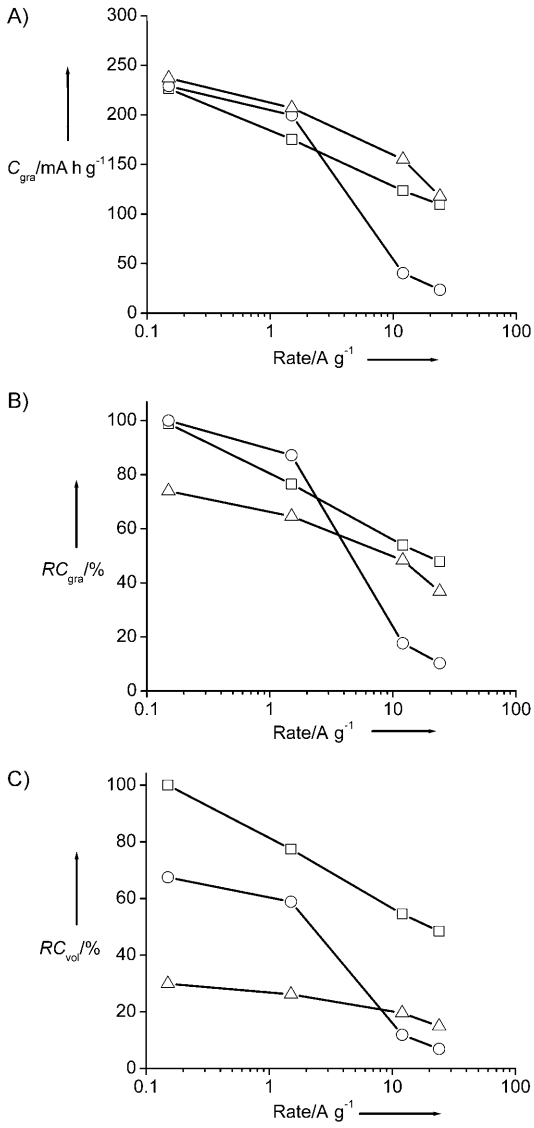

Figure 4. A) Gravimetric capacity retention based on active mass, B) relative gravimetric capacity retention based on total electrode mass (including the mass of carbon and binder), and C) relative volumetric capacity retention based on total electrode volume, for mesoporous anatase (TiO_2:Super S:Kyner = 70:15:15, square), and 6 nm anatase nanoparticle (TiO_2:Super S:Kyner = 70:15:15, circle, and 50:45:5, triangle). C_{gra}: gravimetric capacity; RC_{gra}: relative gravimetric capacity; RC_{vol}: relative volumetric capacity.

the capacities are plotted as a function of increasing rate. Considering first Figure 4a, where the capacities obtained on the first intercalation are normalized by the active mass, it is evident that the nanoparticulate material with 45 wt.% carbon exhibits a capacity that is slightly greater than the mesoporous material with only 15 wt.% carbon throughout the range of rates. However, nanoparticulate anatase with 15 wt.% carbon shows a substantial decrease in capacity at high rates (greater than 1500 $mA\,g^{-1}$). The main conclusion from these results is that the 6 nm particles struggle to maintain satisfactory electron pathways through the electrode compared with the micrometer sized mesoporous materials. Much higher carbon contents are required in the case of the nanoparticulate material in order to exhibit high rate capability. When the capacity is normalized by the total electrode mass (Figure 4b), the mesoporous material exhibits capacities that exceed the nanoparticulate material even with 45 wt.% carbon. Perhaps the most significant result is seen in Figure 4c where the capacity is normalized by the volume of the electrode. Volumetric capacity is increasingly recognized as an important parameter whether for consumer electronics or electric vehicle applications. The electrode volume is obtained directly by measuring the electrode thickness and knowing the electrode area. The mesoporous materials exhibit significantly higher volumetric capacities than the nanoparticulate materials, up to two times higher at the highest rates, despite the lower intrinsic density of mesoporous anatase.

Comparing the behavior of nanoparticle and ordered mesoporous anatase, both exhibit short diffusion distances for Li intercalation (6 nm diameter particles and 6.5 nm thick walls respectively) but:[5]

1. It is difficult to pack nanoparticles efficiently into an electrode while the micrometer sized mesoporous material packs like dense micrometer sized particles.
2. Porosity between the nanoparticles is random in size, some voids being too small for electrolyte ingress and some too large. In the mesoporous phase, the pores are uniform in size and shape, as well as being connected in a continuous 3D network, thus facilitating electrolyte contact and hence maximizing the electrode/electrolyte contact area, without wasting volume.
3. The hierarchical pore structure will aid transport through the electrolyte.
4. More carbon is required to maintain electron pathways to the nm particles than is the case for micrometer sized particles. Carbon coating could be used to more efficiently distribute the conducting additive; although such methods, including the application of redox active molecules or conducting polymer layers, may add some complexity and cost to the electrodes.

The increase in capacity and reversibility that is often observed for two-phase intercalation reactions on moving to the nanoscale is usually attributed to the ease of the two-phase transformation in nanoparticles.[1a,c] However, the mesoporous materials are micrometer sized particles with channels and hence an entire particle cannot transform spontaneously between phases, as has been proposed for nanoparticle anatase and $LiFePO_4$.[1c,3] The nucleation front of a new phase (e.g. the orthorhombic phase that forms on intercalation) must spread across the particle. In the case studied here, the walls of the mesopore are composed of nanodomains of anatase and they could spontaneously switch structures, with strain being relieved at the boundaries between the domains. A related process has been described before for $LiMn_2O_4$ derived from layered $LiMnO_2$.[6] Also the strain of the phase transition is relieved by the thin walls even if though switching of entire particles between phases cannot occur.

Comparing the results for ordered mesoporous anatase with those obtained previously for disordered mesoporous anatase, excellent rate performance was demonstrated in particular by Guo and Maier for the latter when it contained a metallized coating of RuO_2. These elegant studies reported a capacity of 91 $mA\,h\,g^{-1}$ at 10 $A\,g^{-1}$.[7] Interestingly, the ordered mesoporous anatase reported here shows even higher rate performance of 125 $mA\,h\,g^{-1}$ at 12 $A\,g^{-1}$ (35.7 C, Figure S6) without metallization. Of course there may be a number of reasons for these differences and it is difficult to establish clearly the origin without more detailed knowledge of the loading, electrode thickness etc. used in the previous work. However, it does suggest that electron transport (metallizing pore walls), although important, may not be the only rate limiting factor. We suggest that the ordered mesostructure may offer important advantages compared with disordered mesopores in achieving high rate performance. As stated above, all of the pores are of equal size, they are interconnected in a 3D array ensuring equal access of the electrolyte to the entire internal surface of the walls and the walls themselves are all equivalent. These features are not present in disordered mesoporous materials.

In conclusion, we have synthesized an ordered 3D mesoporous anatase using a hard template and investigated lithium intercalation. The structural changes are similar to those observed for nanoparticles, with continuous Li insertion into tetragonal anatase up to $Li_{0.05}TiO_2$, then a two-phase process between anatase and orthorhombic $Li_{0.45}TiO_2$ followed by continuous insertion into the orthorhombic phase up to $Li_{0.96}TiO_2$. Despite the intrinsic porosity of the mesoporous phase, the volumetric capacity is higher than the best results for nanoparticulate anatase reported previously, a two-fold increase being observed at the highest rates (24 $A\,g^{-1}$). The rate capability is better than disordered mesoporous anatase even when the latter is metallized, suggesting that the ordered pore structure is important in achieving high rate capability.

Experimental Section

Preparation of the mesoporous silica (KIT-6) has been described previously.[8] A typical synthesis of mesoporous anatase TiO_2 is as follows: 10 g of titanium oxysulfate (Sigma–Aldrich, Ti $\geq$ 29%, free $H_2SO_4 \leq 17\%$) was dissolved in 50 mL of deionized water. Then the solution was added dropwise to 500 mL of 1 $mol\,L^{-1}$ $NH_3{\cdot}H_2O$ (Aldrich) solution with stirring and a precipitate of white TiO_2 formed. After stirring for 24 h, the mixture was filtered and washed with distilled water. Then the white gel-like precipitation was dissolved in the 15 mL of nitric acid (Aldrich, 70%). Mesoporous

KIT-6 silica was impregnated with an aqueous solution of $TiO(NO_3)_2$ (ca. 2.5 g solution per g KIT-6) using the incipient-wetness method,[9] dried at 60 °C overnight and calcined at 400 °C for 5 h. The resulting material was treated twice with a hot NaOH solution (2 mol L^{-1}) to remove the silica template, followed by washing with water three times and drying at 60 °C for 6 h.

The materials were characterized by TEM (JEOL JEM-2110), wide angle PXRD (Stoe STADI/P diffractometer operating in transmission mode with Fe $K_{\alpha 1}$ radiation, $\lambda = 1.936$ Å), low-angle X-ray diffraction (Rigaku/MSC, D/max-rB with Cu $K_{\alpha 1}$ radiation, $\lambda = 1.541$ Å), and N_2 adsorption (Micromeritics ASAP 2020). The Li intercalated samples were loaded in sealed 0.7 mm glass capillaries in glovebox without contact with the air and moisture before PXRD test.

The in situ Raman data were collected by a Renishaw InVia Raman inverted and upright microscope system (Renishaw, Wotton-under-Edge, UK), equipped with 50/0.5 long working distance objectives. A laser excitation wavelength of 632.8 nm was used, with a filter employed to reduce the laser power to 3 mW at the electrode surface. The setup of the in situ Raman cell has been described previously elsewhere.[1d]

Electrochemical cells were constructed by mixing the active material (anatase), Kynar 2801(a copolymer based on poly(vinylidene fluoride)), and Super S carbon (3M company) in the weight ratio of 70:15:15 if not otherwise specified. The mixture was cast onto copper foil from acetone using the Doctor-Blade technique. After solvent evaporation at room temperature and heating at 80 °C under vacuum for 8 h, the electrodes were assembled into cells with a lithium electrode (99.9 %, Aldrich) and LP-30 electrolyte (Merck; 1 M $LiPF_6$ in 1:1 v/v ethylene carbonate/dimethyl carbonate). The cells were constructed and handled in an argon-filled MBraun glovebox. Electrochemical measurements were carried out using a MACCOR Series 4200 cycler. The 6 nm anatase nanoparticles AMT-100, were supplied by Tayca Corp., Japan. The 15 nm anatase nanoparticles, AK-1, were supplied by Bayer.

Received: December 16, 2009
Published online: March 5, 2010

Keywords: anatase · electrodes · intercalation · lithium batteries · mesoporous materials

[1] a) G. Sudant, E. Baudrin, D. Larcher, J. M. Tarascon, *J. Mater. Chem.* **2005**, *15*, 1263; b) C. H. Jiang, M. D. Wei, Z. M. Qi, T. Kudo, I. Honma, H. S. Zhou, *J. Power Sources* **2007**, *166*, 239; c) M. Wagemaker, W. J. H. Borghols, F. M. Mulder, *J. Am. Chem. Soc.* **2007**, *129*, 4323; d) L. J. Hardwick, M. Holzapfel, P. Novak, L. Dupont, E. Baudrin, *Electrochim. Acta* **2007**, *52*, 5357; e) A. R. Armstrong, G. Armstrong, J. Canales, R. Garcia, P. G. Bruce, *Adv. Mater.* **2005**, *17*, 862; f) G. Armstrong, A. R. Armstrong, J. Canales, P. G. Bruce, *Chem. Commun.* **2005**, 2454.

[2] a) P. G. Bruce, B. Scrosati, J. M. Tarascon, *Angew. Chem.* **2008**, *120*, 2972; *Angew. Chem. Int. Ed.* **2008**, *47*, 2930; b) D. Deng, M. G. Kim, J. Y. Lee, J. Cho, *Energy Environ. Sci.* **2009**, *2*, 818.

[3] C. Delmas, M. Maccario, L. Croguennec, F. Le Cras, F. Weill, *Nat. Mater.* **2008**, *7*, 665.

[4] a) C. Dickinson, W. Z. Zhou, R. P. Hodgkins, Y. F. Shi, D. Y. Zhao, H. Y. He, *Chem. Mater.* **2006**, *18*, 3088; b) A. Rumplecker, F. Kleitz, E. L. Salabas, F. Schüth, *Chem. Mater.* **2007**, *19*, 485; c) F. Jiao, A. H. Hill, A. Harrison, A. Berko, A. V. Chadwick, P. G. Bruce, *J. Am. Chem. Soc.* **2008**, *130*, 5262; d) Y. Ren, F. Jiao, P. G. Bruce, *Microporous Mesoporous Mater.* **2009**, *121*, 90.

[5] Y. Ren, A. R. Armstrong, F. Jiao, P. G. Bruce, *J. Am. Chem. Soc.* **2010**, *132*, 996.

[6] a) P. G. Bruce, A. R. Armstrong, R. L. Gitzendanner, *J. Mater. Chem.* **1999**, *9*, 193; b) A. D. Robertson, A. R. Armstrong, A. J. Fowkes, P. G. Bruce, *J. Mater. Chem.* **2001**, *11*, 113; c) N. Meethong, H. Y. S. Huang, S. A. Speakman, W. C. Carter, Y. M. Chiang, *Adv. Funct. Mater.* **2007**, *17*, 1115; d) M. Tang, H. Y. Huang, N. Meethong, Y. H. Kao, W. C. Carter, Y. M. Chiang, *Chem. Mater.* **2009**, *21*, 1557.

[7] Y. G. Guo, Y. S. Hu, W. Sigle, J. Maier, *Adv. Mater.* **2007**, *19*, 2087.

[8] F. Kleitz, S. H. Choi, R. Ryoo, *Chem. Commun.* **2003**, 2136.

[9] Y. Ren, Z. Ma, L. P. Qian, S. Dai, H. Y. He, P. G. Bruce, *Catal. Lett.* **2009**, *131*, 146.